

# Evolution and sub-surface characteristics of a sea-surface temperature filament and front in the northeastern Arabian Sea during November–December 2012

P. Vipin<sup>a,b</sup>, Kankan Sarkar<sup>a,b</sup>, S. G. Aparna<sup>a,b,\*</sup>, D. Shankar<sup>a,b</sup>, V. V. S. S. Sarma<sup>c,b</sup>,  
D. G. Gracias<sup>a,b</sup>, M. S. Krishna<sup>c</sup>, G. Srikanth<sup>c</sup>, R. Mandal<sup>a,1</sup>, E. P. Rama Rao<sup>d</sup>,  
N. Srinivasa Rao<sup>d</sup>

<sup>a</sup>CSIR-National Institute of Oceanography, Dona Paula, Goa 403004, India.

<sup>b</sup>Academy of Scientific and Innovative Research (AcSIR), CSIR-NIO, Goa, India.

<sup>c</sup>CSIR-National Institute of Oceanography (Regional Centre), Visakhapatnam, India.

<sup>d</sup>ESSO-Indian National Centre for Ocean Information Services, Hyderabad, India.

---

## Abstract

We used satellite-derived sea-surface-temperature (SST) data along with in-situ data collected along a meridional transect between 18.85 and 20.25°N along 69.2°E to describe the evolution of an SST filament and front during 25 November to 1 December in the northeastern Arabian Sea (NEAS). Both features were  $\sim 100$  km long, lasted about a week, and were associated with weak temperature gradients ( $\sim 0.07^\circ\text{C km}^{-1}$ ). The in-situ data were collected first using a suite of surface sensors during a north–south mapping of this transect and showed the existence of a chlorophyll maximum within the filament. This surface data acquisition was followed by a high-resolution south–north CTD (Conductivity-Temperature-Depth) sampling along the transect. In the two days that elapsed between the two in-situ measurements, the filament had shrunk in size and moved northward. In general, the current direction was northwestward and advected these mesoscale features. The CTD data also showed an SST front towards the northern end of the transect. In both these features, the chlorophyll concentration was higher than in the surrounding waters. The temperature and salinity data from the CTD suggest upward mixing or pumping of water from the base of the mixed layer, where a chlorophyll maximum was present, into the mixed layer that was about 60 m thick. A striking diurnal cycle was evident in the chlorophyll concentration, with higher values tending to occur closer to the surface during the night. The in-situ data from both surface sensors and CTD, and so also satellite-derived chlorophyll data, showed higher chlorophyll concentration, particularly at sub-surface levels, between the filament and the front, but there was no corresponding signature in the temperature and salinity data. Analysis of the SST fronts in the satellite data shows that fronts weaker than those associated with the filament and the front had crossed the transect in this region a day or two preceding the sampling of the front.

---

**Keywords.** Mesoscale processes, Frontal systems, Potential Fishery Zones, Indian Ocean, West India Coastal Current.

---

\*

*Email address:* [aparna@nio.org](mailto:aparna@nio.org) (S. G. Aparna)

<sup>1</sup>Present Address: Hind Geophysical Pvt Ltd, Mumbai, India.

## 1. Introduction

Ocean fronts are narrow zones of enhanced horizontal gradients of water properties (for example, temperature) (Belkin et al., 2009; Klein and Lapeyre, 2009). Filaments (also referred to as flumes, tongues, or squirts in the literature) are narrow elongated regions surrounded by water with different properties; the edge of a filament exhibits a curvature (Flament et al., 1985; Haynes et al., 1993). Gradients in water properties are observed at the edges of filaments, and these gradients are often so high that the edges form fronts. An example is seen on the Atlantic coast of the Iberian peninsula, where the edges of upwelling filaments form strong fronts (Haynes et al., 1993). Edges of all filaments need not, however, be fronts. Ramp et al. (1991) showed that a few filaments in the California Current System (Miller et al., 1999) are enclosed by density fronts, but there are filaments that are not bounded by fronts, and the properties change gradually at the edges of these filaments. Off northern California, cold-water filaments have sharp southern and diffuse northern boundaries (Randerson and Simpson, 1993). When we consider a transect across these mesoscale features, we find that gradients are observed only once across a front, implying a monotonic distribution of water properties, but twice across a filament, implying a non-monotonic distribution of properties.

In addition to the gradient in physical properties, both fronts and filaments have chemical and biological manifestations that are reflected in variations in nutrients and chlorophyll (Brink et al., 1998; Belkin et al., 2009). This biogeochemical signature of fronts makes them highly productive (Mackas et al., 1991; Lendt et al., 1999; Etnoyer et al., 2006; Klein and Lapeyre, 2009) and such frontal regions have been exploited for commercial fishing for decades (Laurs et al., 1984; Alemany et al., 2014). Satellite technology, particularly infrared sensors for remote sensing of sea-surface temperature (SST), makes it possible to track such fronts over time (Shaw and Vennell, 2000; Ba and Fablet, 2010), and remote sensing of chlorophyll adds a distinct advantage from the viewpoint of fisheries (Lanz et al., 2009; Solanki et al., 2003a, 2010).

The characteristics of fronts and filaments depend on the region in which they form. In the temperate oceans, the horizontal gradient of properties is high and so is the vertical extent of the feature (Moore et al., 1999; Dong et al., 2006). Cross-frontal differences in SST and sea-surface salinity (SSS) can be as large as 10–15°C and 2–3 psu, respectively; typical differences are of the order of 2–5°C and 0.3–1.0 psu (Belkin et al., 2009). For example, the Florida Current and the Gulf Stream are bordered by two perennial fronts, across which the SST difference ranges between 2–10°C and 1.5–4.5°C, respectively (Belkin et al., 2009). In the Atlantic, filaments off Cape Sao Vicente (Portugal) have a length (width) of about 250 km (50 km) and the temperature difference between the filament and surrounding waters is about 2–3°C (McCreary et al., 1991; Corré and Jesus, 2003). Hickox et al. (2000) studied SST fronts in East China Sea, Yellow Sea, and Bohai Sea and found the cross-frontal SST range upto 4°C, with the fronts exhibiting strong seasonal variability in this region. Apart from such high horizontal gradients, upwelling velocities tend to be higher in a frontal regime (Mahadevan and Tandon, 2006; Klein and Lapeyre, 2009) and enhanced vertical mixing and nutrient flux is observed in the filaments and frontal zones (Niiler et al., 1989; Johnston et al., 2011). Observations show that the vertical extent is  $\sim 75$  m for the Kuroshio Front (Park and Chu, 2006) and  $\sim 100$ –150 m for the Agulhas Front (Belkin and Gordon, 1996).

In the tropical oceans, SST fronts or filaments with such high gradients are observed only in the regime of strong western-boundary currents and upwelling zones (Evans and Brown, 1981). In the north Indian Ocean (NIO), a long, persistent frontal system in the Gulf of Aden adjoining the Arabian Sea shows a cross-frontal temperature difference of  $\sim 5^\circ\text{C}$  during the summer monsoon (Belkin et al., 2009), when strong upwelling is forced off both Somalia (to the south of the gulf) and Oman (to the north of the gulf) (Wyrтки, 1971; McCreary et al., 1993). A temperature difference of  $\sim 6^\circ\text{C}$  was observed across an upwelling front along the west

coast of India, during the summer monsoon in 1987 (Unnikrishnan and Antony, 1992). Often associated with such strong temperature fronts are long filaments (see, for example, Lierheimer and Banse (2002) and the review by Hood et al., 2009). In general, the temperature gradients tend to be weaker in the tropics and the temperature difference was just  $1^{\circ}\text{C}$  across cold-water filaments observed during the summer monsoon off Somalia in 1997 (Lendt et al., 1999) and Oman in 1995 (Barber et al., 2001). In the southeastern Arabian Sea (SEAS), Maheshwaran et al. (2000) observed SST fronts at the surface and at 50 m; the cross-frontal gradient was  $\sim 0.02^{\circ}\text{C km}^{-1}$ , an order of magnitude smaller than in the temperate oceans. A similar gradient was observed in a transect in the Bay of Bengal off the east coast of India (Hareesh et al., 2013); the transect sampled across two fronts during December 1997 and January 1998, and the cross-frontal temperature gradient was just  $0.07^{\circ}\text{C km}^{-1}$ . The vertical extent of these fronts was also smaller, ranging from 25 m to 40 m.

In spite of the much weaker temperature gradients observed across tropical fronts and filaments, the link between such mesoscale fronts or filaments and fisheries in the temperate oceans (see, for example, Laurs and Burcks, 1985; Maul et al., 1984; Alemany et al., 2014) has inspired their use for commercial fisheries in India (Narendranath et al., 1991; Solanki et al., 1998c, 2001a, 2003a, 2008; Mahadevan, 2014), and SST fronts, along with satellite chlorophyll data, have been used to delineate Potential Fishery Zones (PFZs) in the Indian Exclusive Economic Zone (EEZ) (Zainuddin and Saitoh, 2004; Solanki et al., 2001b, 2005). The PFZ advisories are issued by the Indian National Centre for Ocean Information Services (INCOIS; <http://www.incois.gov.in/>). Studies suggest that the fish catch in a PFZ is higher than in a non-PFZ (Solanki et al., 2003b; Choudhary et al., 2007; Deshpande et al., 2011). Economic analyses suggest that the PFZ advisories reduce the cost of fishing (Nayak et al., 2003), implying that the ephemeral SST fronts associated with these PFZs have a commercial value.

Most of the studies on such fronts in the NIO are either confined to the surface (owing to the use of only satellite data) (Belkin et al., 2009), or represent a few hydrographic sections that sampled across these features (Unnikrishnan and Antony, 1992; Maheshwaran et al., 2000; Hareesh et al., 2013), or report fish catch within and outside a designated PFZ (Solanki et al., 2003b, 2005; Choudhary et al., 2007; Deshpande et al., 2011). Yet, between the formation of an SST front or filament, which is a *surface* physical feature that can be discerned in satellite data, and the fish that lie at the apex of the marine food web is an intricate web of chemical and biological processes that determine the evolution of the complex marine ecosystem. In order to gain insight into the ecosystem dynamics underlying the PFZs, an inter-disciplinary programme called OCEAN FINDER was launched by the CSIR-National Institute of Oceanography in 2012. One task under this programme is collecting and analysing data, across a host of disciplines, on transects across such SST fronts. As noted by Hopkins et al. (2010), to capture the evolution of these mesoscale features as they “grow, merge, split, shrink, and disappear” over a short span of time, typically a week, is a challenge as fronts and filaments invariably represent nonlinear flows and processes over a range of different temporal and spatial scales. Our plan therefore was to determine the contour of a front or filament in satellite SST data and run a transect perpendicular to the front. Given that the cross-frontal spatial scale is small, the transect is expected to be short, of the order of just 100 km. Though these mesoscale features are seen practically all over the NIO, their concentration is not uniform in space and time.

A cruise in the eastern Arabian Sea was allotted to this programme during 23 November to 11 December 2012. Analysis of daily and 3-day averages of MODIS (Moderate Resolution Imaging Spectroradiometer) Aqua SST data (see Table 1 for the data sources) for November–December during 2008–2011 showed that fronts are more ubiquitous in the northeastern Arabian Sea (NEAS) during this period (Figure 1). Obenour (2014) analysed 30 years of SST data and showed that the average probability of a clear pixel (no clouds) and of the existence of a front

is also higher in the NEAS than in other regions of the NIO.

Hence, we decided to carry out the cruise in the NEAS, which is an interesting laboratory for studying the coupling between physics and ecosystem dynamics even on spatial scales much larger than those associated with the mesoscale SST fronts. This region is highly productive owing to surface cooling by dry continental winds that lead to convective mixing during the winter monsoon (Banse, 1968; Shetye et al., 1992). This winter cooling deepens the mixed layer, entraining nutrients into it, and leading to high productivity (Banse, 1984; Madhupratap et al., 1996; McCreary et al., 2009). As a result of the evaporation associated with this winter cooling, the salinity is higher at the surface in the NEAS. The vertical profile of salinity shows four salinity extrema (Rochford, 1964; Shenoi et al., 1993).

This paper describes the physical aspects of a Filament and a Front that were sampled during the cruise in November–December 2012. (Capitalisation, i. e., use of *Filament* or *Front*, implies a reference to *the* filament or front; when referring to other filaments or fronts, or to filaments and fronts in general, we use the small case.) We use satellite data to describe the evolution of the fronts in the region of interest during the cruise, and use data collected using a surface-sensor system and a CTD (Conductivity-Temperature-Depth) to describe the variability of temperature, salinity, and chlorophyll. The paper is organised as follows. Section 2 describes the data and methods, including the cruise plan. The evolution of the filament and front, as seen in satellite data, is described in Section 3. Section 4 describes the variation along a transect as mapped by the surface sensors, and Section 5 the variation mapped using a CTD. Section 6 concludes the paper.

## 2. Data and Methods

Prior to the cruise, we had access only to the data that were available online from MODIS Aqua (Table 1). These data had a temporal resolution of one day and a spatial resolution of 4 km; to plan the cruise, we used these daily data and also their three-day averages owing to the several gaps in the daily data set. For the post-cruise analysis, we found these temporal resolutions inadequate to interpret the in-situ observations and therefore used the Level-2 SST data archived at INCOIS. These AVHRR (Advanced Very-High-Resolution Radiometer) SST data, from MetOp-B, NOAA-18, and NOAA-19 (NOAA: National Oceanic and Atmospheric Administration) satellites (Table 1), have a spatial resolution of 1 km and a temporal resolution of 12 hours (two passes, one each during day and night), implying the availability of six SST images per day because these satellites pass over the NEAS at different times of the day. Though these data also have gaps, the transect covered during the cruise was not affected much by them.

To map the SST fronts, we used the algorithm of Cayula and Cornillon (1992). This algorithm uses a cutoff for the mean temperature difference between the two populations on either side of the front; the default value of  $0.375^{\circ}\text{C}$ , used by Ullman and Cornillon (2000) for the northwest Atlantic, was too high for the weaker SST gradients in the NEAS. Therefore, we used a cutoff of  $0.15^{\circ}\text{C}$ . This parameter has also been relaxed in some earlier studies: for example, Wall (2006) used a cutoff of  $0.125^{\circ}\text{C}$  on the west Florida shelf. For the front-detection sensitivity parameter, however, we used the default value of 0.76 (Cayula and Cornillon, 1992) because a relaxation to 0.72, as done by Wall (2006), led to too many weak fronts. The filaments were identified by analysing both SST contours and SST fronts.

Analysis of the daily and 3-day-average data showed that most of the fronts and filaments in the NEAS are oriented zonally, suggesting that a meridional transect was more likely to sample across them. (This orientation preference was subsequently confirmed with the high-resolution data sets.) The cruise plan was dictated by this fact and that communication with the vessel, *RV Sindhu Sankalp*, was restricted to radio telephone: the vessel did not have access to the Internet or email during this cruise, implying that the transect could not be changed at will based on

the latest satellite maps. The vessel sailed from Mormugao port in Goa, west coast of India (see Figure 1) on 23 November; the last communication of a satellite image to the vessel was made on 25 November at 16:30 hours IST (Indian Standard Time, which is 5.5 hours ahead of UTC), when the vessel came within the range for mobile communication off the coast of Gujarat, India. Subsequently, all decisions were based on the in-situ observations. Based on the satellite data, we decided to run a meridional transect at 69.2°E from  $\sim 19$ –20°N, but the end points of the transect were to be fixed on the basis of the in-situ data. This meridian was chosen because an ADCP (acoustic Doppler current profiler) mooring was available at (69.2°E, 19.98°N) (Amol et al., 2014).

The vessel first ran a transect at 69.2°E from 20.50–18.85°N with a towed suite of surface sensors. The entire transect, mapped at a speed of  $\sim 3$  knots (5.5 km per hour) from north to south, started on 26 November at 0200 IST and ended on 28 November at 0140 IST. (Note that the local time at this longitude is 53.2 minutes behind IST.) This towed sensor suite, assembled locally, consisted of a SeaBird portable CTD, which had sensors for detecting temperature, conductivity and pressure (depth), and additional sensors for chlorophyll, nitrate, and photosynthetically available radiation (PAR), and a fast-repetition-rate fluorometer. This sensor system was mounted on one side of the ship and was towed at a depth of about seven metres to ensure that it did not surface in spite of the rolling and pitching. In this paper, we report only the temperature, salinity, and chlorophyll data (Figure 3).

Following the completion of this north–south transect with the surface sensors, the transect was resampled from south to north with a CTD being deployed at 42 stations over this distance of  $\sim 140$  km; the CTD transect was truncated at 20.25°N and we therefore show the in-situ data only for 18.85–20.25°N. This CTD transect started on 28 November at 1045 IST and ended on 1 December at 0540 IST. The station spacing was roughly one nautical mile (NM; 1 NM equals 1.8 km) when the in situ data indicated the existence of a front or filament. The CTD used was a SeaBird 911Plus with sensors for detecting temperature, conductivity, pressure, chlorophyll, PAR, and sound velocity; as with the surface-sensor system, we restrict our attention in this paper to temperature, salinity, and chlorophyll. The CTD chlorophyll, measured with a WetLabs sensor emitting (absorbing) at 470 (695) nanometres, is highly correlated ( $r = 0.88$ ; Rajdeep Roy, personal communication) with the chlorophyll measured using HPLC (high-performance liquid chromatography); the pigment HPLC data are reported in Roy et al. (2015). The CTD casts were made to a depth of 500 m, but we report here only the data for the top 100 m because the mixed layer and the sub-surface chlorophyll maximum (Cullen, 1982; Banse, 1987) that lies at its base and is characteristic of the Arabian Sea (Brock et al., 1993), were within this depth range. The downcast to 100 m took about four minutes, during which the drift of the vessel was less than 0.00038 NM, much less than even the 1 NM station interval near a front. Therefore, the downcast data can be considered to provide a vertical profile at the location of the CTD cast; these stations are marked in Figure 3. Water samples were collected at 22 of these 42 stations on the upcast; these chemical and biological data form the subject of other papers.

We have also used satellite chlorophyll data that were available online from MODIS Aqua (Table 1). These chlorophyll data had a temporal resolution of one day and spatial resolution of 4 km, but the data showed large gaps. For example, during the week starting 25 November and ending 1 December, when the Filament and Front were mapped during the cruise, data were available on the transect for just four days.

The other data we have used are currents from the ADCP mooring (Amol et al., 2014), surface currents from the OSCAR (Ocean Surface-Current Analysis Real-time) data set (Bonjean and Lagerloef, 2002), ASCAT wind data on board MetOp-A, and rainfall data from the TRMM’s (Tropical Rainfall Measuring Mission) TMI (TRMM Microwave Imager). Data sources are listed in Table 1.

### 3. Satellite Data

We used 12-hourly SST data from MeTop-B, NOAA-18, and NOAA-19 satellites to track the evolution of a cold-water Filament and a Front (Figure 2). These mesoscale features were  $\sim 100$  km long and their signatures are seen in the CTD data and the Filament is seen in the surface-sensor data as well.

The front associated with the Filament, denoted by the red contour in Figure 2, was first seen in the NEAS on 25 November, with cooler (warmer) waters to its north (south); the temperature difference across the front was just  $\sim 0.2^\circ\text{C}$ . This front warped over the next two days, with its northern part moving northwestward even as the southern part remained practically stationary. By 27 November, the front had acquired sufficient curvature for the Filament to form: the cooler waters were enclosed by the warmer waters and the temperature difference had increased to  $\sim 0.3^\circ\text{C}$ . The size and shape of the Filament changed with time. On average, it shrank in size, i. e., its width at  $69.2^\circ\text{E}$  decreased from  $\sim 30$  km on 27 November to  $\sim 10$  km on 29 November. This decrease in width was largely due to the northward movement of the southern edge of the Filament (refer to the rectangle with black, dashed edges in Figure 2). On 30 November, SST decreased by  $\sim 1^\circ\text{C}$  all over the NEAS and the Filament was not seen (even when the cutoffs in the Cayula and Cornillon (1992) algorithm were lowered); clouding on this day in the region implied that only one of the six satellite images had useful data. The Filament was seen again on 1 December, when the clouds disappeared, but the SST gradient weakened thereafter and the Filament disappeared by 2 December. Since this part of the transect was mapped with the surface sensors on 28 November and with the CTD on 29 November, the structure of the Filament is seen in both in-situ data sets (Figure 3).

The Front, denoted by the magenta contour in Figure 2, was first seen in the region shown in Figure 2 on 22 November and it moved northwestward. As with the Filament, its shape changed over time and it first crossed the transect on 28 November, intersecting it at  $19.5^\circ\text{N}$ . The vessel, then mapping the transect from north to south with the surface sensors, had already moved further south and the Front was therefore not detected in these surface data (Figure 3). The SST changes ensured that the Front had shrunk in length on 29 November and was not detectable on 30 November (Figure 2). By 1 December, however, the clouds had disappeared and, in spite of the cooling of the NEAS, the SST gradients had recovered and the Front was seen again: it intersected the transect at  $\sim 20.10^\circ\text{N}$ , leading to its structure being mapped by the CTD (Figure 3).

The satellite chlorophyll data (see the bottom row of Figure 2) show that the concentration, which was  $\sim 0.2$   $\text{mg m}^{-3}$  near the front associated with the Filament on 26 November, decreased marginally by 28 November, but was practically constant thereafter. The peak concentration of  $\sim 0.6$   $\text{mg m}^{-3}$  occurred near the northern end of the Front, but it was matched by the peak seen between the Filament and the Front on 26 and 28 November and 1 December; in between, on 29 November, the chlorophyll concentration in this part of the transect was lower (Figure 2 and second panel of Figure 3).

### 4. Spatial variability at the surface

The surface sensor system showed little variation in SST ( $\sim 27.30^\circ\text{C}$ ) and sea surface salinity (SSS;  $\sim 36.30$  psu or practical salinity unit) from the northern end of the transect to  $\sim 19.6^\circ\text{N}$ , southward of which the SST and SSS started increasing (Figure 3). The SST (SSS) increased to  $27.6^\circ\text{C}$  (36.60 psu) at  $19.4^\circ\text{N}$ , but then decreased to  $\sim 27.35^\circ\text{C}$  ( $\sim 36.40$  psu) in the regime of Filament. The SST (SSS) increased again to  $27.75^\circ\text{C}$  (36.60 psu) at  $19.23^\circ\text{N}$ . The SST and SSS gradients at the northern and southern boundaries of the Filament were low: the SST (SSS) gradient was  $0.025^\circ\text{C km}^{-1}$  ( $0.015$  psu  $\text{km}^{-1}$ ) at the northern boundary and  $0.030^\circ\text{C km}^{-1}$

( $0.012 \text{ psu km}^{-1}$ ) at the southern boundary. Within the Filament, the SST and SSS gradients were even lower. Southward of the southern boundary of the Filament, the SST hardly varied till the end of the transect, but the salinity decreased gradually to 36.40 psu. As noted above, the Front moved over the transect only after the vessel had moved south of its southern limit.

A chlorophyll peak was seen in the northern part of this SST Filament. The concentration was  $\sim 0.1 \text{ mg m}^{-3}$  to the south of the Filament, but increased within it, reaching a peak of  $0.7 \text{ mg m}^{-3}$  (Figure 3). Though the chlorophyll concentration decreased immediately north of the Filament, it increased again between  $19.45\text{--}19.6^\circ\text{N}$ , with two peaks of 0.6 and  $0.5 \text{ mg m}^{-3}$  in this regime. The chlorophyll concentration decreased to  $0.2\text{--}0.3 \text{ mg m}^{-3}$  north of  $19.6^\circ\text{N}$ , but it increased again north of  $19.95^\circ\text{N}$ . We do not have satellite chlorophyll data for 27 November, when most of the transect was mapped using the surface sensors, but the data for 26 and 28 November show similar chlorophyll peaks north of the Filament. We discuss these additional chlorophyll peaks, which do not have a Front or Filament analogue in the SST and SSS data, in Section 6.

In these surface data, the width of the Filament (defined as the distance within which the SST and SSS values remained low and the horizontal gradient of SST and SSS was negligible in comparison even to the weak gradients at the boundaries of the Filament) was  $\sim 20 \text{ km}$  (Figure 3), much less than the  $\sim 30 \text{ km}$  estimated from satellite data (Figure 2), but the southern boundary of the Filament in the two data sets was the same ( $19.23^\circ\text{N}$ ). A possible reason for this discrepancy lies in the details of the SST fronts within the regime of the Filament. As seen in the satellite data of 0130 IST on 28 November, another, weaker front ran almost parallel to the  $69.2^\circ\text{E}$  meridian from the northern limit of the Filament to  $\sim 19.40^\circ\text{N}$ . A closer examination of these in-situ SST data shows that the northern limit of the Filament in these data lies close to the latitude of intersection of this front and the transect (Figure 2). Note that a difference in position is to be expected because the two measurements are not simultaneous and the fronts move quite rapidly, as can be seen by the difference in this region between the two SST images for 28 November (see the panels for 0130 and 0330 IST). If the northern limit of the Filament in the surface-sensor data is considered to be the small peak in SST that is seen at  $\sim 19.50^\circ\text{N}$ , then the width of the Filament increases to  $\sim 30 \text{ km}$ , which is comparable to the satellite-based estimate.

## 5. The CTD section

Both mesoscale features, the Filament and the Front, were seen in the CTD section that was run from south to north.

Temperature in the southern part of the CTD transect was  $\sim 27.8^\circ\text{C}$  in the surface mixed layer, which was  $\sim 60 \text{ m}$  deep (Figure 3). (The mixed layer depth was calculated following Shenoi et al. (2004), which defined it as the depth at which  $\sigma_t$  exceeds that at the surface by the increase in  $\sigma_t$  that would be caused by a  $1^\circ\text{C}$  change in temperature.) Salinity in this part of the transect increased from 36.40 psu at the southern end to 36.50 psu, with patches of higher salinity also seen. Both temperature and salinity started decreasing in the afternoon of 29 November at  $\sim 19.37^\circ\text{N}$ , marking the southern boundary of the Filament, which had moved north from its location as estimated from the surface-sensor suite during the night of 27 November. As may be expected from the decrease in the width of the Filament from 27 to 29 November in the satellite data (Figure 2), the width of the Filament estimated from the CTD section was  $\sim 10 \text{ km}$  at the surface. The Filament was funnel-shaped in the temperature and salinity vertical sections and its width decreased to  $\sim 5 \text{ km}$  at the base of the mixed layer (Figure 3). The lowest value of temperature (salinity) measured by the CTD within the Filament was  $27.20^\circ\text{C}$  (36.40 psu). This minimum in temperature and salinity within the Filament matched the lower temperature and salinity at the base of the mixed layer (Figure 3) that is characteristic of the eastern Arabian

Sea (Rochford, 1964; Shenoi et al., 1993). Indeed, the CTD data suggest that water from the base of the mixed layer is pumped into the mixed layer in the regime of the Filament. The temperature and salinity in the core of the Filament were lower than that at its boundaries, and the horizontal gradients of temperature and salinity at the boundaries were comparable to the SST and SSS gradients measured earlier using the surface sensors. Near the southern boundary of the Filament, where the sampling was done in the afternoon, a diurnal mixed layer about 10–15 m deep was evident in the temperature profile. This diurnal mixed layer, which disappeared in the northern part of the Filament because it was sampled in the late evening and night, is seen more clearly in the zoomed image of the section shown in Figure 4 to highlight the variation within the Filament.

Both temperature and salinity increased north of the Filament, the exception being a slightly cooler ( $\sim 27.0^\circ\text{C}$ ) patch with SSS as low as  $\sim 36.10$  psu at  $\sim 19.55^\circ\text{N}$ ; this patch was just  $\sim 15$  m deep and the mixed layer was shallowest in its vicinity. Temperature and salinity decreased again around  $\sim 20.10^\circ\text{N}$ , marking the southern boundary of the Front, which extended northward till the end of the transect. One significant difference between the Filament and the Front is the warm ( $\sim 27.40^\circ\text{C}$ ), high-salinity ( $\sim 36.50$  psu) layer about  $\sim 20$  m thick, in the latter that separated the cooler and fresher surface mixed layer from the salinity minimum below the mixed layer. The SSS in the northern half of the Front, around  $\sim 20.20^\circ\text{N}$ , was even lower ( $\sim 36.0$  psu), and the mixed layer, estimated using a density criterion, was therefore just  $\sim 15$  m thick in this part of the transect. Both temperature and salinity tended to increase at the northernmost station.

Striking in the chlorophyll data on the transect was the higher concentration at the base of the mixed layer (Figure 3), which is characteristic of the Arabian Sea (Marra and Barber, 2005). In the mixed layer, the chlorophyll concentration was low ( $\sim 0.10$  mg m $^{-3}$ ) to the south of the Filament, but increased within it (Figure 3). Its vertical profile, however, did not show the funnel shape evident in temperature and salinity. While the base of the chlorophyll peak practically coincided with that of the temperature and salinity minima in the Filament, the peak of  $\sim 0.80$  mg m $^{-3}$  in the upper half of the mixed layer was shifted about 4 km to the north. This meridional shift in the chlorophyll peak within the mixed layer appears to be due to the diurnal cycle: the peak is nearer the surface during the night and shifts down within the mixed layer during the day (Figure 4). This decrease in the near-surface CTD chlorophyll during the day is often attributed to non-photochemical quenching (see, for example, Poll et al., 2011), but this process is ruled out in this case because the decrease is also seen in pigment data (Figures 4 and 5 of Roy et al., 2015).

Chlorophyll concentration was high in the regime of the Front as well, but the concentration in the Front was lower than in the Filament even though the temperature and salinity were higher in the latter (Figure 3). The highest concentration in the Front,  $\sim 0.60$  mg m $^{-3}$ , was observed during the night of 1 December. The concentration estimated from satellite data that day was higher in this part of the Front, but much lower than the CTD estimate in the regime of the Filament on 29 November (second panel of Figure 3).

The chlorophyll concentration was not affected by the patch of low salinity around  $\sim 20.20^\circ\text{N}$  in the northern part of the Front: instead, the chlorophyll concentration showed a decrease only in the high-salinity tongue, suggesting that the biological response was not affected by the low-salinity patch within the Front, just as it was unaffected by the low-salinity patch around  $\sim 19.55^\circ\text{N}$ .

As in the surface-sensor data, the chlorophyll concentration did not decrease as dramatically to the north of the Filament as it did to its south. Unlike temperature and salinity, which did not show any sub-surface signature between the Filament and the Front, there were patches between the Filament and the Front in which chlorophyll concentration was elevated above the minimum



seen in this regime of the transect and to the south of the Filament. The higher chlorophyll concentration in these patches between the Filament and the Front did not, however, extend to the surface (except between 19.90–20.00°N) and, therefore, would not have been seen in a surface-sensor tow had it been carried out during 29–30 November. The satellite data also show a decrease in the chlorophyll concentration between the Filament and the Front from 26 or 28 November to 29 November (Figure 3). The higher chlorophyll concentration in this region seen in the surface-sensor tow during 27 November was restricted largely to sub-surface levels just two days later. We discuss these chlorophyll patches in Section 6.

## 6. Discussion

We have used satellite (Figure 2) and in-situ data (Figure 3) along a meridional transect from 18.85–20.25°N at 69.2°E to describe the evolution of a filament and a front in the NEAS. Both mesoscale features lasted about a week, and, as is typical of such features in the region, were associated with a weak temperature gradient of  $\sim 0.04\text{--}0.08^\circ\text{C km}^{-1}$ . The salinity gradient was  $\sim 0.02\text{--}0.05$  psu  $\text{km}^{-1}$ . The chlorophyll concentration, measured in situ, was higher (0.5–0.9  $\text{mg m}^{-3}$ ) in the regimes of the Filament and the Front than in the surrounding waters.

The satellite data show that the Front moved northwestward during 25 November to 1 December (Figure 5). The OSCAR current (Bonjean and Lagerloef, 2002) was northwestward during this week, suggesting advection of the Front across the NEAS. Comparison with direct measurements with an ADCP (Amol et al., 2014) show that the OSCAR current at  $\sim 20^\circ\text{N}$  captures well the seasonal cycle of the observed variability of the alongshore component of the West India Coastal Current (WICC) (Shankar and Shetye, 1997; Shankar et al., 2002), but there are significant differences at the intraseasonal periods that matter in the context of the Front; the correlation at this ADCP location is also weaker for the cross-shore component (Amol et al., 2014). Since the OSCAR data are available at an interval of five days, the errors are likely to be larger when we consider the movement of a front that lasts but a week. Comparison with ADCP data for November–December 2012 (Figure 5), the period of the cruise, shows that the OSCAR current is in the same direction as the ADCP current, but the negligible temporal variability in the OSCAR current is in sharp contrast to the considerable variation in the magnitude of the ADCP current even within this short period.

This smoothness in the temporal variability of the OSCAR current extends to the spatial variation (Figure 5). Given the differences between the ADCP vector and the OSCAR vectors in Figure 5, one can expect greater spatial variability at short length scales than is seen in the OSCAR data. This short-scale variability is indicated in the more complex changes seen in the shape of the filament during the week: the northern part of the filament does move north westward, but its southern part does not move as much, and its shape changes much more than is possible if the current field were as uniform as in the OSCAR data. Note that the winds during this week were from the north (Figure 5); while they could have contributed to the westward component of the current via Ekman drift, the direct influence of winds on the movement of fronts, as suggested by Vinuchandran et al. (2004), was not evident in these data.

Nevertheless, the OSCAR data do provide a first-order approximation to the large-scale WICC, and we used them to investigate the causes of the low-salinity surface patches seen in the CTD section around 19.55°N and 20.20°N (Figure 3). Using the OSCAR currents to compute a Lagrangian trajectory backward in time allowed us to trace the origin of these patches to high-rainfall events ( $> 20$  mm over a day) seen in the TMI data at an earlier time (Figure 6). The patch observed at 19.55°N on 29 November was traced to a rainfall event at (69.90°E, 16.50°N) on 22 October and the patch observed at 20.20°N on 1 December to an event at (71.20°E, 19.00°N) on 1 November. While it is possible that the OSCAR current speed of 10–20  $\text{cm s}^{-1}$  is an underestimate, this Lagrangian computation suggests that high-rainfall events can create

low-salinity patches that can survive over a month as they are advected by the local currents. Such long-distance advection of low-salinity patches has been reported earlier from the central part of the Indian west coast (Shankar et al., 2005), but the CTD data suggest that these patches need not have a chlorophyll signature (Figure 3). We note here that the salinity signal in these patches is  $\sim 0.5$  psu and they could not be traced in the data available from Aquarius (Table 1) (Menezes et al., 2014).

The other shallow feature in the CTD section is the thin diurnal mixed layer about 15 m thick. Such a thin diurnal mixed layer is seen within the Filament and between the Filament and the Front (Figure 3). The diurnal cycle was evident in the chlorophyll as well, with higher concentration seen closer to the surface during the day and away from the surface during the night. A diurnal cycle of chlorophyll was reported earlier for the northcentral Arabian Sea during the winter monsoon (Prasanna Kumar et al., 2001) and this chlorophyll diurnal cycle has been attributed to a diurnal cycle in the depth of the mixed layer (Wiggert et al., 2002), which seems to be driven by the diurnal wind field (McCreary et al., 2001, 2009). In our CTD data, however, the diurnal cycle was not seen in the salinity field and was too weak to affect the depth of the mixed layer (Figure 3).

More interesting is the chlorophyll signature between the Filament and the Front because there is no corresponding signature in the temperature and salinity (Figure 3). Similar signatures of chlorophyll at the surface, without a corresponding signature in SST or SSS, were also seen in the surface-sensor data collected before the CTD transect (Figure 3). Since the fronts move, i. e., are advected by the currents, water moves away from a given location and leaves behind no signature in the temperature or salinity field. Yet, there is a biological signature at the location. A possible reason for this chlorophyll signature lies in the evolution of SST and SST fronts. Note that the chlorophyll concentration was low in the southern part of the transect, over which practically no frontal activity was seen since 25 November (see the bottom panel of Figure 3). A few weak fronts crossed the transect in this regime on 25 and 27 November and 1 December, and an increase in the CTD chlorophyll concentration was seen at sub-surface levels in this region around 18.9°N on 28 November, a day on which no frontal activity was noted in this region. Likewise, several fronts, though weaker than those mapped as the Filament and the Front, crossed the transect between these features in the days before it was mapped using the surface sensors or the CTD. We speculate that this history of frontal activity is important for the ecosystem. If this hypothesis is correct, an implication is that chlorophyll may not coincide with an SST front seen in satellite data: there can be chlorophyll at or below the surface owing to the history of frontal activity at a given location. Signatures of this chlorophyll that survives the movement of a front are seen in the satellite data as well (second panel of Figure 3), but the spatial resolution of the MODIS chlorophyll is coarser than that achieved in the in-situ measurements reported in this paper.

What can cause this biological signature to be present when the physical signature is advected away? This is one of the questions that emerge from this study. Another question concerns the physical mechanism leading to these fronts and filaments. The CTD data, particularly from the regime of the Filament (Figure 3), suggest that water is pumped or mixed upward into the mixed layer from its base. Though the horizontal temperature gradients are weak in the tropics and in the data presented in this paper, it is possible that the weak upwelling velocities associated with them (Mahadevan and Tandon, 2006; Klein and Lapeyre, 2009) are sufficient to pump water from the base of the mixed layer into it. Modelling studies suggest that surface blooms can occur in the Bay of Bengal as a consequence of the entrainment of a sub-surface bloom (chlorophyll maximum) into the mixed layer (Vinayachandran, 2009). If the water from the base of the mixed layer is pumped into it, will the species that determine the higher chlorophyll concentration at the base of the mixed layer be the same as those populating the mixed layer

in the regime of the fronts? Pigment data from this cruise show that the population in the chlorophyll maximum at the base of the mixed layer is not the same as in the Filament or Front (Roy et al., 2015), implying more complex ecosystem processes are at work than may be suggested by simple ecosystem models.

The satellite data for the NEAS suggest that the high chlorophyll concentration seen in the region study is linked to processes on the shelf, where the concentration is even higher (Figure 7). It is possible that filaments can break out of the shelf during bursts in the cross-shore component of the WICC. Such current bursts are evident in the ADCP data during November–December 2012 (Figure 5) and seem to occur frequently during winter off the Indian west coast (Amol et al., 2014). A similar connection of fronts to shelf processes has been noted elsewhere too (Haynes et al., 1993; Strub et al., 1991; Smyth et al., 2001) and deserves further study.

In summary, we have reported an increase in chlorophyll concentration in the regime of a front and a filament along one transect in the NEAS. In the California Current System, major SST fronts have been shown to be always associated with chlorophyll fronts (Kahru et al., 2012). Therefore, a useful question is whether an SST front in the NEAS, or in the rest of the north Indian Ocean, will always be linked to chlorophyll. In other words, is the existence of an SST front, if the gradient associated with it is above some yet unidentified threshold, a sufficient condition for an increase in chlorophyll concentration? If the answer to this question is positive, then what are the time scales associated with the evolution of the ecosystem associated with a front? How does the ecosystem evolve as the front warps and moves over time? In other words, what is the link between a “major” SST front off the west coast of India and the locations identified in advisories on potential fishery zones, which motivated this study of the frontal systems?

Most studies of biophysical coupling in the north Indian Ocean have been restricted to the large spatial scales and the seasonal cycle or interannual variability associated with major climate modes (see the reviews by Hood et al., 2009; McCreary et al., 2009; Vinayachandran, 2009; Konè et al., 2009; Marra and Moore, 2009; Wiggert et al., 2009) because observations at these shorter scales have not been available (McCreary et al., 2009). Modelling studies do suggest, however, that mesoscale processes do contribute to the nutrient budgets in the Arabian Sea (Resplandy et al., 2011) and that sub-mesoscale fronts that last but a few days can arise owing to instabilities of the mesoscale currents (Lévy et al., 2012). The data presented in this paper constitute the first report of a high-resolution CTD transect across a mesoscale frontal system in the north Indian Ocean; the data also show more ephemeral, sub-mesoscale fronts between the Filament and Front that dominate the transect and suggest that they have an influence on the biology. Answering the questions that arise even from this limited survey demands a sustained interdisciplinary observational and modelling programme to map and understand the biophysical variability at the spatial and temporal scales associated with these mesoscale features.

## Acknowledgements

This study was funded by the OCEAN FINDER (PSC 0105) programme of CSIR-NIO. We thank S. R. Shetye for inspiring this inter-disciplinary programme, S. S. C. Shenoi for his keen interest and encouragement, and A. C. Anil and other OCEAN FINDER colleagues for their patience as our ideas about the cruise data evolved over several months. A. C. Anil also helped with the biological aspects of the background for this paper. We are grateful to Peter Cornillon for prompt assistance when we faced problems with the Cayula and Cornillon (1992) algorithm, to the master and his officers and crew on board *RV Sindhu Sankalp* for their assistance during the cruise, to the ship cell of CSIR-NIO for support, to S. Vernekar and T. Ramesh for technical assistance during the cruise, to Ashok Kankonkar for help in processing the CTD data, and to Rajdeep Roy, Rajath Chitari, K. R Mangala, Vinayak Kulkarni, Niyathi Hede, E. Ranjith, and N. Anil Kumar for their support throughout the cruise. The possibility of non-photochemical quenching being responsible for the decrease in near-surface chlorophyll was pointed out by an anonymous reviewer of an earlier version of the manuscript. P. Vipin and K. Sarkar acknowledge the University Grants Commission and Council of Scientific and Industrial Research, respectively for financial support; both also acknowledge the Academy of Scientific and Innovative Research (AcSIR). This is NIO contribution 5757.

## References

- Aleman, D., Acha, E. M., Iribarne, O. O., 2014. Marine fronts are important fishing areas for demersal species at the Argentine Sea (Southwest Atlantic Ocean). *Journal of Sea Research* 87, 56–67.
- Amol, P., Shankar, D., Fernando, V., Mukherjee, A., Aparna, S. G., Fernandes, R., Michael, G. S., Khalap, S. T., Satelkar, N. P., Agarvedekar, Y., Gaonkar, M. G., Tari, A. P., Kankonkar, A., Vernekar, S. P., 2014. Observed intraseasonal and seasonal variability of the West India Coastal Current on the continental slope. *Journal of Earth System Science* 123, 1045–1074.
- Ba, S. O., Fablet, R., 2010. Variational fronts tracking in sea surface temperature images. *Proceedings of 2010 IEEE 17th International Conference of Image Processing*. pp. 4117–4120.
- Banse, K., 1968. Hydrography of the Arabian Sea shelf of India and Pakistan and effects on demersal fishes. *Deep-Sea Research* 15, 45–79.
- Banse, K., 1984. Overview of the hydrography and associated biological phenomena in the Arabian Sea, off Pakistan. *Marine Geology and Oceanography of Arabian Sea and Coastal Waters*. B.U. Huq & J.D. Milliman (eds.) Van Nostrand Reinhold Co., N.Y., 271–303.
- Banse, K., 1987. Clouds, deep chlorophyll maxima and the nutrient supply to the mixed layer of stratified bodies. *Journal of Plankton Research* 9, 1031–1036.
- Barber, R. T., Marra, J., Bidigare, R. C., Codispoti, L. A., Halpern, D., Johnson, Z., Latasa, M., Goericke, R., Smith, S. L., 2001. Primary productivity and its regulation in the Arabian Sea during 1995. *Deep-Sea Research II* 48, 1127–1172.

- Belkin, I. M., Cornillon, P. C., Sherman, K., 2009. Fronts in Large Marine Ecosystems. *Progress in Oceanography* 51, 223–236.
- Belkin, I. M., Gordon, A. L., 1996. Southern Ocean fronts from the Greenwich meridian to Tasmania. *Journal of Geophysical Research* 101, 3675–3696.
- Bell, C., Vassie, J. M., Woodworth, P. L., 1998. *POL – PSMSL Tidal Analysis Software Kit 2000 (TASK – 2000)*, Permanent Service for Mean Sea Level. Proudman Oceanographic Laboratory, UK.
- Bonjean, F., Lagerloef, G. S. E., 2002. Diagnostic Model and Analysis of the Surface Currents in the Tropical Pacific Ocean. *Journal of Physical Oceanography* 32, 2938–2954.
- Brink, K., Arrone, R. A., Coble, P., Flagg, C., Jones, B., Kindle, J., Lee, C., Phinney, D., Wood, M., Yentsch, C., Young, D., 1998. Monsoons boost biological productivity in Arabian sea. *EOS Transactions American Geophysical Union* 79, 165–169.
- Brock, J., Sathyendranath, S., Platt, T., 1993. Modelling the seasonality of subsurface light and primary production in the Arabian Sea. *Marine Ecology Progress Series* 101, 209–211.
- Cayula, J., Cornillon, P. C., 1992. Edge Detection Algorithm for SST Images. *Journal of Atmospheric and Oceanic Technology* 9, 67–80.
- Choudhary, S. B., Jena, B., Rao, M. V., Rao, K. H., Somvanshi, V. S., Gulati, D. K., Sahu, S. K., 2007. Validation of integrated potential fishing zone (IPFZ) forecast using satellite based chlorophyll and sea surface temperature along the east coast of India. *International Journal of Remote Sensing* 28, 2683–2693.
- Corré, V., Jesus, S. M., 2003. Tracking cold water upwelling filaments in the ocean using matched-field inversion. *Acta Acustica united with Acustica* 89, 604–613.
- Cullen, J. J., 1982. The Deep Chlorophyll Maximum: Comparing Vertical Profiles of Chlorophyll a. *Canadian Journal of Fisheries and Aquatic Sciences* 39, 791–803.
- Deshpande, S. P., Radhakrishnan, K. V., Bhat, U. G., 2011. Direct and Indirect Validation of Potential Fishing Zone Advisory off the Coast of Uttara Kannada, Karnataka. *Journal of Indian Society of Remote Sensing* 39, 547–554.
- Dong, S., Gille, S. T., Sprintall, J., Gentemann, C., 2006. Validation of the Advanced Microwave Scanning Radiometer for the Earth Observing System AMSR-E sea surface temperature in the Southern Ocean. *Journal of Geophysical Research* 111, C04002.
- Etnoyer, P., Canny, D., Mate, B. R., Morgan, L. E., Ortiz, J. G. O., Nichols, W., 2006. Sea-surface temperature gradients across blue whale and sea turtle foraging trajectories off the Baja California Peninsula, Mexico. *Deep-Sea Research II* 53, 340–358.
- Evans, R. H., Brown, O. B., 1981. Propagation of thermal fronts in the Somali Current System. *Deep Sea Research Part A. Oceanographic Research Papers* 28, 521–527.
- Flament, P., Armi, L., Washburn, L., 1985. The evolving structure of an upwelling filament. *Journal of Geophysical Research* 90, 11765–11778.
- Hareesh, P. V., Mathew, B., Kumar, M. R. R., Rao, A. R., Jagadeesh, P. S. V., Radhakrishnan, K. G., Shyni, T. N., 2013. 'Thermohaline front' off the east coast of India and its generating mechanism. *Ocean Dynamics* 63, 1175–1180.

- Haynes, R., Barton, E. D., Pilling, I., 1993. Development, Persistence and Variability of Upwelling filaments off the Atlantic Coast of the Iberian Peninsula. *Journal of Geophysical Research* 98, 22681–22692.
- Hickox, R., Belkin, I. M., Cornillon, P. C., Shan, Z., 2000. Climatology and seasonal variability of ocean fronts in the East China, Yellow and Bohai Seas from satellite SST data. *Geophysical Research Letters* 27, 2945–2948.
- Hood, R. R., Wiggert, J. D., Naqvi, S. W. A., 2009. Indian Ocean Research: Opportunities and Challenges. *Geophysical Monograph Series* 185, 409–428.
- Hopkins, J., Challenor, P., Shaw, A. G. P., 2010. A New Statistical Modeling approach to ocean front detection from SST Satellite images. *Journal of Atmospheric and Oceanic Technology* 27, 173–191.
- Johnston, T. M. S., Rudnick, D. L., Sanz, E., 2011. Elevated mixing at a front. *Journal of Geophysical Research* 116, C11033, doi:10.1029/2011JC007192.
- Kahru, M., Lorenzo, E. D., Sarabia, M. M., Mitchell, B. G., 2012. Spatial and temporal statistics of sea surface temperature and chlorophyll fronts in the California Current. *Journal of Plankton Research* 34, 749–760.
- Klein, P., Lapeyre, G., 2009. The Oceanic Vertical Pump Induced by Mesoscale and Submesoscale Turbulence. *Annual Review of Marine Science* 1, 351–375.
- Konè, V., Aumount, O., Lèvy, M., Resplandy, L., 2009. Physical and Biogeochemical Controls of the Phytoplankton Seasonal Cycle in the Indian Ocean: A Modeling Study. *Geophysical Monograph Series* 185, 147–166.
- Lanz, E., Martínez, J. L., Martínez, M. N., Dworak, J. A., 2009. Small pelagic fish catches in the Gulf of California associated with sea surface temperature and chlorophyll. *CalCOFI Report* 50, 134–146.
- Laurs, R. M., Burcks, J. T., 1985. Living marine resources applications. *Advances in Geophysics* 27, 419–452.
- Laurs, R. M., Fiedler, P., Montgomery, D., 1984. Albacore tuna catch distributions relative to environmental features observed from satellites. *Deep-Sea Research* 31, 1085–1099.
- Lendt, R., Hupe, A., Ittekkot, V., Bange, H. W., Andreae, M. O., Thomas, H., Habsi, S. A., Rapsomanikis, S., 1999. Greenhouse gases in cold water filaments in the Arabian Sea during Southwest Monsoon. *Naturwissenschaften* 86, 489–491.
- Lévy, M., Ferrari, R., Franks, P. J. S., Martin, A. P., Rivière, P., 2012. Bringing physics to life at the mesoscale. *Geophysical Research Letters* 39, doi:10.1029/2012GL05276, L14602.
- Lierheimer, L. J., Banse, K., June 2002. Seasonal and interannual variability of phytoplankton pigment in the Laccadive (Lakshadweep) Sea as observed by the coastal zone color scanner. *Proceedings of the Indian Academy of Sciences, Earth and Planetary Sciences, Indian Academy of Sciences*, 111, 163–185.
- Mackas, D. L., Washburn, L., Smith, S. L., 1991. Zooplankton community pattern associated with a California Current cold filament. *Journal of Geophysical Research* 96, 2515–2534.

- Madhupratap, M., Prasanna Kumar, S., Bhattathiri, P. M. A., Raghukumar, S., Nair, K. K. C., Ramaiah, N., 1996. Mechanism of biological response to winter cooling in the northeastern Arabian Sea. *Letters to Nature* 384, 549–552.
- Mahadevan, A., 2014. Ocean science: Eddy effects on biogeochemistry. *Nature* 506, 168–169.
- Mahadevan, A., Tandon, A., 2006. An analysis of mechanisms for submesoscale vertical motion at ocean fronts. *Ocean Modelling* 14, 241–256.
- Maheshwaran, P. A., Rajesh, G., Revichandran, C., Nair, K. K. C., 2000. Upwelling and associated hydrography along the west coast of India during southwest monsoon, 1999. The Fifth Pacific Ocean Remote Sensing Conference (PORSEC), 5-8 December 2000 2, 873–878.
- Marra, J., Barber, R. T., 2005. Primary productivity in the Arabian Sea: A synthesis of JGOFS data. *Progress in Oceanography* 65, 159–175.
- Marra, J., Moore, T. S., 2009. Monsoons, Islands, and Eddies: Their Effects on Phytoplankton in the Indian Ocean. *Geophysical Monograph Series* 185, 57–70.
- Maul, G. A., Roffer, M., Sousa, F. M., 1984. Remotely sensed oceanographic patterns and variability of blue fin tuna catch in the Gulf of Mexico. *Oceanologica Acta* 7, 469–479.
- McCreary, J. P., Fukamachi, Y., Kundu, P. K., 1991. A numerical investigation of Jets and Eddies near an eastern ocean boundary. *Journal of Geophysical Research* 96, 2515–2534.
- McCreary, J. P., Kohler, K. E., Hood, R. R., Smith, S., Kindle, J., Fischer, A. S., Weller, R. A., 2001. Influences of diurnal and intraseasonal forcing on mixed-layer and biological variability in the central Arabian Sea. *Journal of Geophysical Research* 106, 7139–7155.
- McCreary, J. P., Kundu, P. K., Molinari, R. L., 1993. A numerical investigation of dynamics, thermodynamics and mixed-layer processes in the Indian Ocean. *Progress in Oceanography* 31, 181–244.
- McCreary, J. P., Murtugudde, R., Vialard, J., Vinayachandran, P. N., Wiggert, J. D., Hood, R. R., Shankar, D., Shetye, S. R., 2009. Biophysical Processes in the Indian Ocean. *Geophysical Monograph Series* 185, 9–32.
- Menezes, V. V., Vianna, M. L., Phillips, H. E., 2014. Aquarius sea surface salinity in the South Indian Ocean: Revealing annual-period planetary waves. *Journal of Geophysical Research: Oceans* 119, 3883–3908.
- Miller, A. J., McWilliams, J. C., Schneider, N., Allen, J. S., Barth, J. A., Beardsley, R. C., Chavez, E. P., Chereskin, T. K., Edwards, C. A., Haney, R. L., Kelly, K. A., Kindle, J. C., Ly, L. N., Moisan, J. R., Noble, M. A., Niiler, P. P., Oey, L. Y., Schwing, F. B., Shearman, R. K., Swenson, M. S., 1999. Observing and Modeling the California Current System. *EOS Transactions AGU* 80, 533–539.
- Moore, J. K., Abbot, M. R., Richman, J. G., 1999. Location and dynamics of the Antarctic polar front from satellite sea surface temperature data. *Journal of Geophysical Research* 104, 3059–3073.
- Narendranath, A., M. V. Rao, S. R. R., Das, N. K., Baral, N., 1991. Application of satellite derived sea surface temperature of estimation of fish catch; A pilot study. *Indian Journal of Marine Sciences* 20, 152–154.

- Nayak, S., Solanki, H. U., Dwivedi, R. M., 2003. Utilization of IRS P4 ocean colour data for potential fishing zone – A cost benefit analysis. *Indian Journal of Marine Sciences* 32, 244–248.
- Niiler, P. P., Poulain, P. M., Haury, L. R., 1989. Synoptic three-dimensional circulation in an onshore-flowing filament of the California Current. *Deep Sea Research II* 36, 385–405.
- Obenour, K. M., 2014. Temporal trends in global sea surface temperature fronts. Open Access Master's Theses.
- Park, S., Chu, P. C., 2006. Thermal and Haline Fronts in the Yellow/East China Seas: Surface and Subsurface Seasonality Comparison. *Journal of Oceanography* 62, 617–638.
- Poll, W., Lagunas, M., T.Vries, Visser, R. W., Buma, A., 2011. Non-photochemical quenching of chlorophyll fluorescence and xanthophylls cycle responses after excess par and uvr in *chaetoceros brevis*, *phaeocystis antarctica* and coastal antarctic phytoplankton. *Marine Ecology Progress Series* 426, 119–131.
- Prasanna Kumar, S., Ramaiah, N., Gauns, M., Sarma, V. V. S. S., Muraleedharan, P. M., Raghukumar, S., Kumar, M. D., Madhupratap, M., 2001. Physical forcing of biological productivity in the Northern Arabian Sea during the Northeast Monsoon. *Deep-Sea Research II* 48, 1115–1126.
- Raja, B. T. A., 1964. Some aspects of spawning biology of Indian oil sardine *Sardinella longiceps Valenciennes*. *Indian Journal of Fisheries* 11A(1), 45–120.
- Ramp, S. R., Jessen, P. F., Brink, K. H., Niiler, P. P., Daggett, F. L., Best, J. S., 1991. The Physical Structure of Cold Filaments Near Point Arena, California, during June 1987. *Journal of Geophysical Research* 96, 14859–14883.
- Randerson, J. T., Simpson, J. J., 1993. Recurrent Patterns in surface thermal fronts associated with cold filaments along the west coast of North America. *Remote Sensing of Environment* 46, 146–163.
- Resplandy, L., Lévy, M., Madec, G., Pous, S., Aumont, O., Kumar, D., 2011. Contribution of mesoscale processes to nutrient budgets in the Arabian Sea. *Journal of Geophysical Research* 116, doi:10.1029/2011JC007006, C11007.
- Rochford, D. J., 1964. Salinity maxima in the upper 1000 meters of the north Indian Ocean. *Australian Journal of Marine and Freshwater Research* 15, 1–24.
- Roy, R., Rajath, C., Vinayak, K., Krishna, M. S., Sarma, V. V. S. S., Anil, A. C., 2015. CHEMTAX-derived phytoplankton community structure associated with temperature fronts in the northeastern Arabian sea. *Journal of Marine Systems* 144, 81–91.
- Shankar, D., Shenoi, S. S. C., Nayak, R. K., Vinayachandran, P. N., Nampoothiri, G., Almeida, A. M., Michael, G. S., Ramesh Kumar, M. R., Sundar, D., Sreejith, O. P., 2005. Hydrography of the eastern Arabian Sea during summer monsoon 2002. *Journal of Earth System Science* 114, 459–474.
- Shankar, D., Shetye, S. R., 1997. On the dynamics of the Lakshadweep high and low in the southeastern Arabian sea. *Journal of Geophysical Research* 102, 12551–12562.
- Shankar, D., Vinayachandran, P. N., Unnikrishnan, A. S., 2002. The monsoon currents in the North Indian Ocean. *Progress in Oceanography* 52, 63–120.



- Sharma, G. S., 1968. Seasonal variation of some hydrographic properties of the shelf waters off the west coast of India. *Bulletin of National Institute of Sciences of India*. 38, 263–276.
- Shaw, A. G. P., Vennell, R., 2000. A front-following algorithm for AVHRR SST imagery. *Remote Sensing of Environment* 72, 317–327.
- Shenoi, S. S. C., Shankar, D., Shetye, S. R., 2004. Remote forcing annihilates barrier layer in southeastern Arabian Sea. *Geophysical Research Letters* 31, L05307, doi:10.1029/2003GL019270.
- Shenoi, S. S. C., Shetye, S. R., Gouveia, A. D., Michael, G. S., 1993. Salinity extrema in the Arabian Sea. *Monsoon Biogeochemistry* (eds.) V. Ittekkot and R. R. Nair, Mitt. Geol.-Palaontol. Inst. Univ. Hamburg 76, 37–49.
- Shetye, S. R., Gouveia, A. D., Shenoi, S. S. C., 1992. Does winter cooling lead to the subsurface salinity minimum off Saurashtra, India. *Oceanography of the Indian Ocean*, 617–625.
- Smyth, T. J., Miller, P. I., Groom, S. B., Lavender, S. J., 2001. Remote sensing of sea surface temperature and chlorophyll during Lagrangian experiments at the Iberian margin. *Progress in Oceanography* 51, 269–281.
- Solanki, H. U., Dwivedi, R. M., Nayak, S. R., 2001a. Synergistic analysis of Sea WiFS chlorophyll and NOAA–AVHRR derived SST features for marine living resources. *International Journal of Remote Sensing* 22, 3877–3882.
- Solanki, H. U., Dwivedi, R. M., Nayak, S. R., 2001b. Application of Ocean Colour Monitor chlorophyll and AVHRR SST for fishery forecast: Preliminary results off Gujarat coast, north-west coast of India. *Indian Journal of Marine Science* 30, 132–138.
- Solanki, H. U., Dwivedi, R. M., Nayak, S. R., 2003a. Application of remotely sensed closely coupled biological and physical process for marine fishery resources exploration. *Journal of Society of Indian Remote Sensing* 31, 67–70.
- Solanki, H. U., Dwivedi, R. M., Nayak, S. R., Somvanshi, V. S., Gulati, D. K., Pattnayak, S. K., 2003b. Fishery forecast using OCM chlorophyll concentration and AVHRR SST: Validation results off Gujarat Coast, India. *International Journal of Remote Sensing* 24, 3691–3699.
- Solanki, H. U., Mandoki, P. C., Nayak, S. R., Somvanshi, V. S., 2005. Evaluation of remote-sensing-based potential fishing zones (PFZs) forecast methodology. *Continental Shelf Research* 25, 2163–2173.
- Solanki, H. U., Mankodi, P. C., Dwivedi, R. M., Nayak, S. R., 2008. Satellite observation of main oceanographic processes to identify ecological associations in the Northern Arabian Sea for fishery resources exploration. *Hydrobiologia* 612, 269–279.
- Solanki, H. U., Prakash, P., Dwivedi, R. M., Nayak, S., Kulkarni, A., Somvamshi, V. S., 2010. Synergistic application of oceanographic variables from multi-satellite sensors for forecasting potential fishing zones: methodology and validation results. *International Journal of Remote Sensing* 31, 775–789.
- Solanki, H. U., Raman, M., Kumari, B., Dwivedi, R. M., Narain, A., 1998c. Seasonal trends in the fishery resources off Gujarat: Salient observation using NOAA–AVHRR. *Indian Journal of Marine Sciences* 27, 438–442.

- Strub, P. T., Kosro, P. M., Huyer, A., 1991. The Nature of the Cold Filaments in the California Current System. *Journal of Geophysical Research* 96, 14743–14768.
- Ullman, D. S., Cornillon, P. C., 2000. Evaluation of front detection methods for satellite-derived sst data using in situ observations. *Journal of Atmospheric and Oceanic Technology* 17, 1667–1675.
- Unnikrishnan, A. S., Antony, M. K., 1992. On an upwelling front along the west coast of India during later part of southwest monsoon. *Physical Processes in the Indian Seas*, 131–135.
- Vinayachandran, P. N., 2009. Impact of physical processes on chlorophyll distribution in the Bay of Bengal; Indian Ocean biogeochemical processes and ecological variability. *Geophysical Monograph Series* 185, 71–86.
- Vinuchandran, R., Solanki, H. U., Dwivedi, R. M., Nayak, S., Jeyaram, A., Adiga, S., 2004. Studies on the drift of ocean color features using satellite-derived sea surface wind for updating potential fishing zone. *Indian Journal of Marine Science* 33, 122–128.
- Vivekanandan, E., Narayanakumar, R., Najmudeen, T. M., Jayasankar, J., Ramachandran, C., 2010. Seasonal fishing ban. *Marine Fisheries Policy Brief - 2* 103, 1–44.
- Wall, C., 2006. Linkages between environmental conditions and recreational king mackerel catch off west-central florida. *Theses and Dissertations Paper* 2743.
- Wiggert, J. D., Murtugudde, R. G., McClain, C. R., 2002. Process controlling interannual variations in wintertime (Northeast Monsoon) primary productivity in the central Arabian Sea. *Deep-Sea Research II* 49, 2319–2343.
- Wiggert, J. D., Vialard, J., Behrenfeld, M. J., 2009. Basin-wide modification of dynamical and biogeochemical processes by the positive phase of the Indian Ocean Dipole during the seaWiFS era. *Geophysical Monograph Series* 185, 385–407.
- Wyrtki, K., 1971. *Oceanographic Atlas of the International Indian Ocean Expedition*. National Science Foundation, Washington, D. C.
- Zainuddin, M., Saitoh, S. I., 2004. Detection of potential fishing ground for albacore tuna using synoptic measurements of ocean color and thermal remote sensing in the northwestern North Pacific. *Geophysical Research Letters* 31, L20311, doi:10.1029/2004GL021000.

## Tables

Table 1: Data sets and their sources. The first column lists the data source and the sensor (when applicable, in parentheses), the second column the variable measured or estimated, the third column the resolution of the data, and the fourth column the Internet resource from which the data were downloaded. In the third column, the first number gives the temporal resolution (in days) and the second number (in parentheses) the spatial resolution (in km). Note that Aquarius carries three radiometers and one scatterometer operating at 1.4 GHz and 1.2 GHz, respectively. The radiometer data are used along with SST data collected by other satellites to derive surface salinity. The OSCAR current represents an average over the top 30 m of the water column. AVHRR: Advanced Very-High-Resolution Radiometer.

Data Source (Sensor)	Variable	Resolution	URL
Aqua (MODIS)	SST	1 (4)	<a href="http://oceandata.sci.gsfc.nasa.gov/">http://oceandata.sci.gsfc.nasa.gov/</a>
Aqua (MODIS)	Chlorophyll	1 (4)	<a href="http://oceandata.sci.gsfc.nasa.gov/">http://oceandata.sci.gsfc.nasa.gov/</a>
NOAA-18 (AVHRR-3)	SST	0.5 (1)	
NOAA-19 (AVHRR-3)	SST	0.5 (1)	
MetOp-B (AVHRR-3)	SST	0.5 (1)	
MetOp-A (ASCAT)	Wind	1 (25)	<a href="http://www.ifremer.fr/cersat/en/data/data.html">www.ifremer.fr/cersat/en/data/data.html</a>
Aquarius	SSS	7 (100)	<a href="http://podaac.jpl.nasa.gov/aquarius/">http://podaac.jpl.nasa.gov/aquarius/</a>
OSCAR	Current	5 (36)	<a href="http://podaac.jpl.nasa.gov/dataset/OSCAR.L4.OC.third-deg/">http://podaac.jpl.nasa.gov/dataset/OSCAR.L4.OC.third-deg/</a>
TRMM (TMI)	Rainfall	1 (4)	<a href="http://trmm.gsfc.nasa.gov/">http://trmm.gsfc.nasa.gov/</a>

## Figures

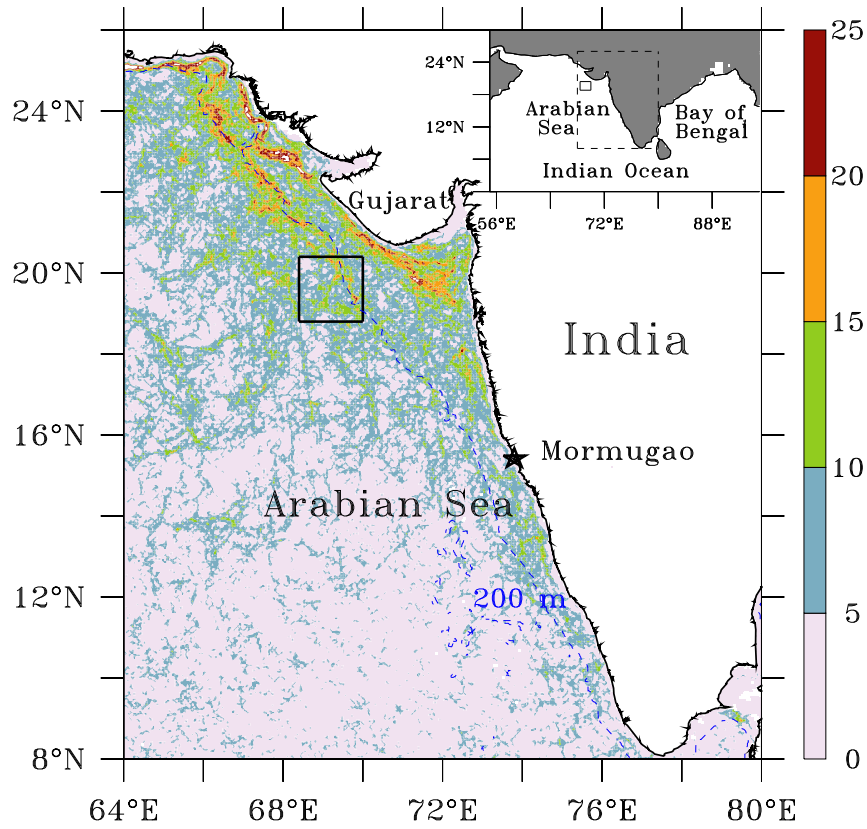


Figure 1: Number of occurrences of a front in a  $4 \text{ km} \times 4 \text{ km}$  pixel in the Arabian Sea during November–December. The fronts were mapped using data for 2008–2011. The blue dashed curve shows the 200 m isobath marking the shelf break and the black box shows the region depicted in the panels in Figure 2. The inset shows the larger region around that shown in the figure.

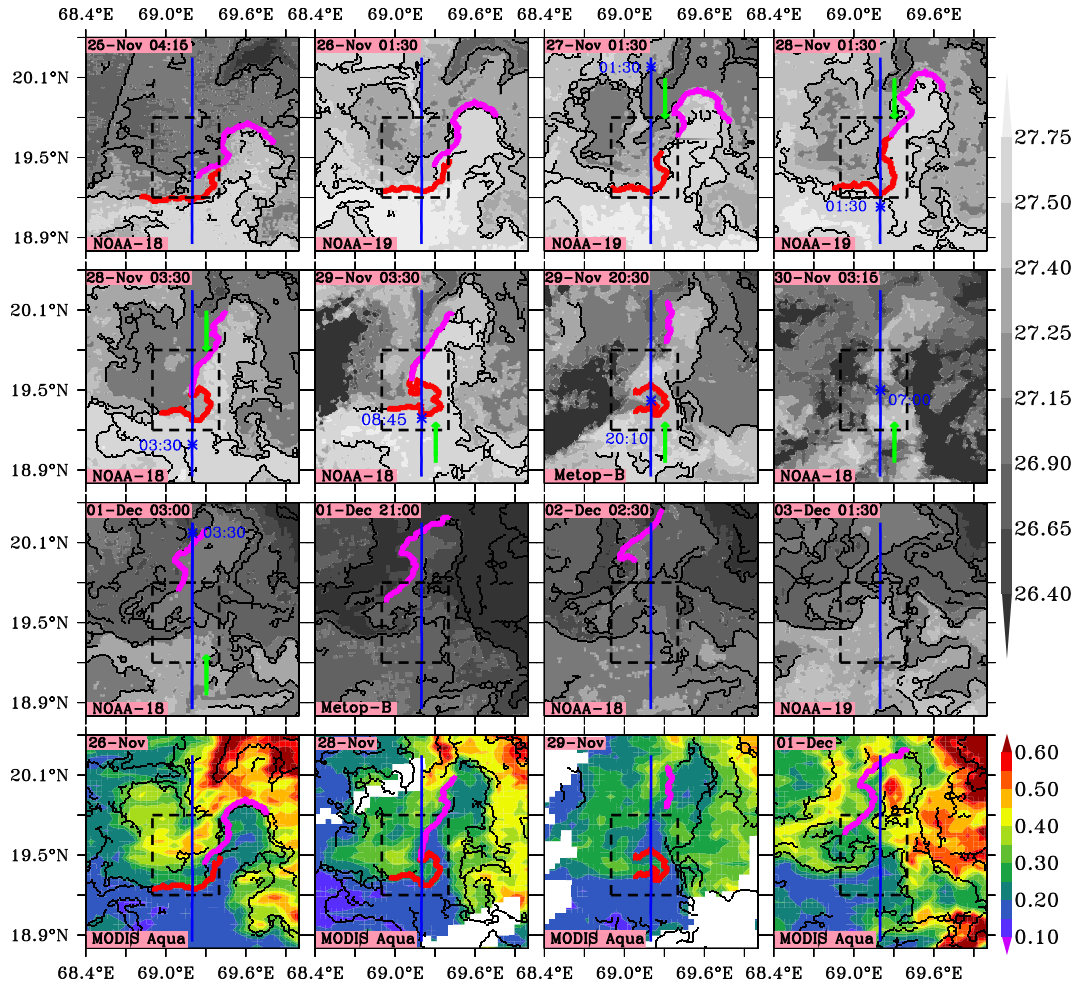


Figure 2: Satellite SST ( $^{\circ}\text{C}$ ) images (first three rows) during 25 November to 3 December 2012, illustrating the formation of the Filament (denoted by the red curve) and the Front (denoted by the magenta curve). Other fronts are denoted by black curves. The date and time of the satellite pass is written in the top left corner of each panel and the name of the satellite in the lower left corner. The blue line shows the cruise track and the green arrows show the direction of movement of the vessel at the time of the satellite pass. The vessel moved southward during 27–28 November and northward during 28 November to 1 December. In each panel, the blue asterisk, if present, marks a CTD sampling location along with the time. The box marked with black dashed lines is drawn to emphasise the northward movement and shrinking of the filament. The fourth row shows chlorophyll ( $\text{mg m}^{-3}$ ) features from MODIS Aqua, with SST fronts overlaid on them, on four days during this week.

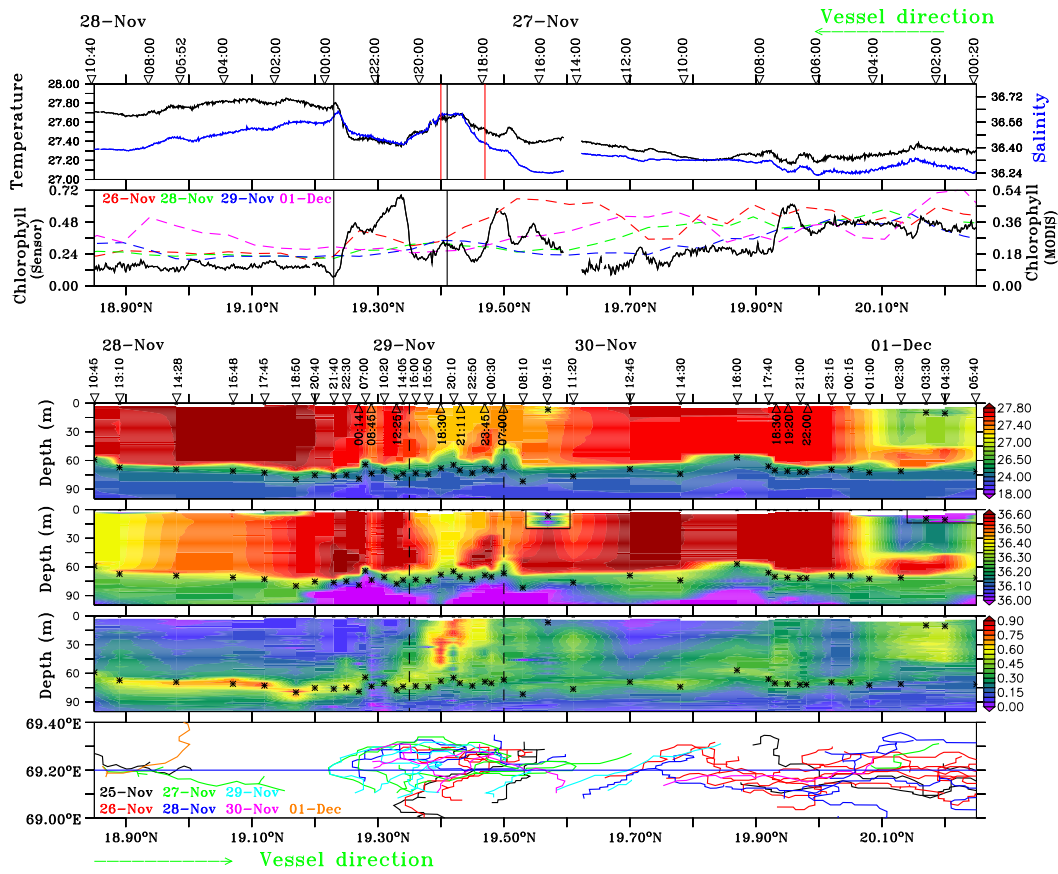


Figure 3: SST ( $^{\circ}\text{C}$ ) and SSS (psu) (first panel from the top) and chlorophyll ( $\text{mg m}^{-3}$ ) measured using the surface-sensor system towed north–south along the transect (second panel). The coloured curves in the second panel are for the MODIS Aqua chlorophyll data. The inverted triangles marked on the top axis of the top panel indicate the location of the vessel at the given time (IST). The vertical black lines in these two panels mark the boundaries of the Filament, as seen in the surface-sensor data on 27 November, and the red lines mark the boundaries of the Filament as seen in the CTD data on 29 November. The vertical profiles of temperature ( $^{\circ}\text{C}$ , third panel), salinity (psu, fourth panel), and chlorophyll ( $\text{mg m}^{-3}$ , fifth panel) measured during the CTD transect show that the Filament narrowed and moved northward over these two days. The sampling locations and time are marked by inverted triangles on the top axis of the temperature panel (third from top). The black asterisks in these three panels denotes the base of the surface mixed layer. The vertical black dashed lines in these panels mark the part of the transect shown in Figure 4 and the rectangles with black edges mark the low-salinity patches that were observed on this transect; these patches are discussed in Section 6. The bottom panel marks the fronts seen from 25 November to 1 December. Note the movement of fronts across the transect (marked by a blue line at  $69.2^{\circ}\text{E}$ ) between the Filament and the Front in the days preceding the surface-sensor and CTD transects. The direction of movement of the vessel, north–south (south–north) for the surface-sensor (CTD) measurements, is indicated by the green arrows.

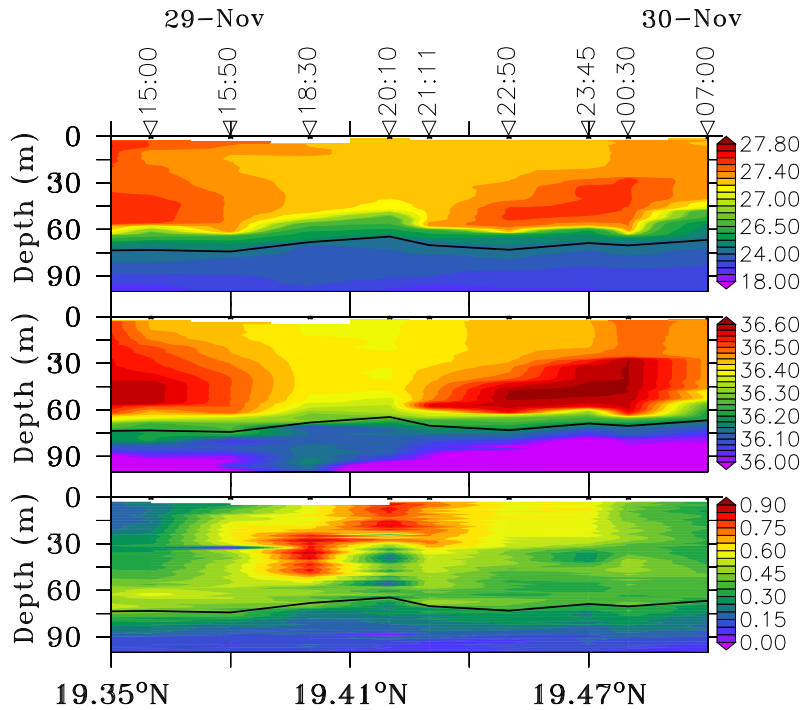


Figure 4: A zoomed image of the vertical profile of temperature ( $^{\circ}\text{C}$ , top panel), salinity (psu, middle panel), and chlorophyll ( $\text{mg m}^{-3}$ , bottom panel) from the CTD transect during 29–30 November 2012. This figure, showing the part of the transect marked by the vertical black dashed lines in Figure 3, highlights the diurnal cycle: note the thin thermal mixed layer in the temperature panel and the upward shift of the chlorophyll maximum within the filament during the night.

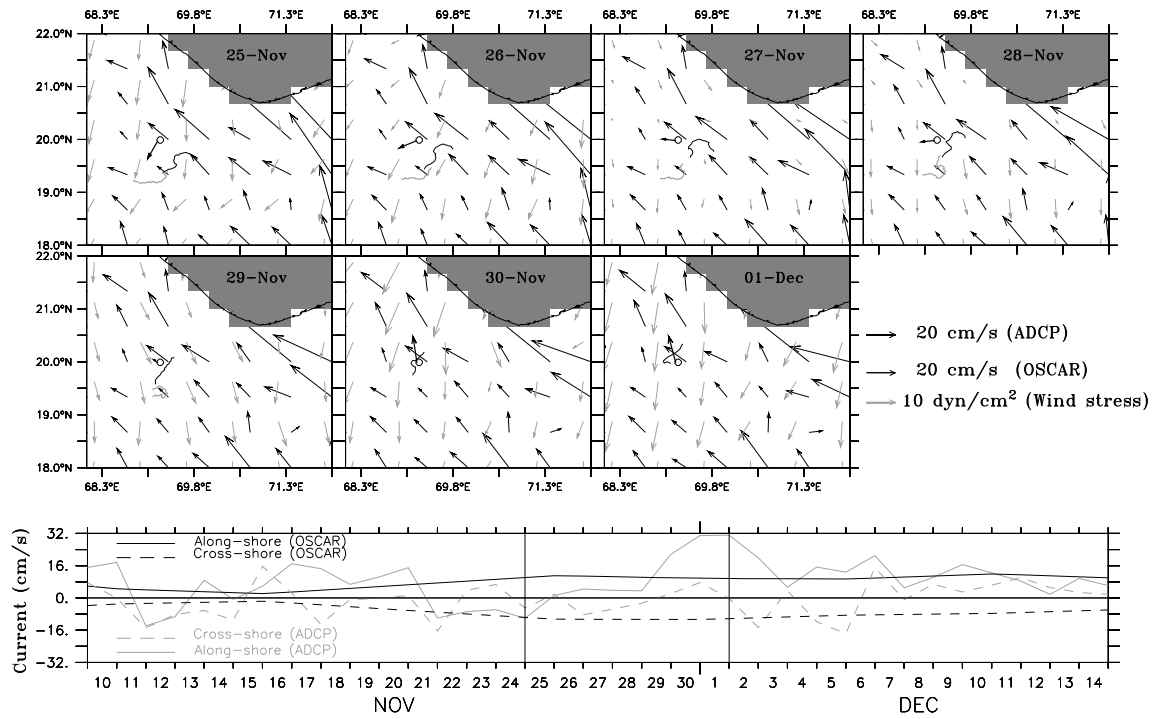


Figure 5: The seven panels in the first two rows show the Filament (grey curve) and the Front (black curve) during 25 November to 1 December. Superimposed on these curves are current vectors from OSCAR (thin black arrows) and the ADCP mooring at ( $69.2^{\circ}\text{E}$ ,  $19.98^{\circ}\text{N}$ ) (one thick black arrow in each panel, with the mooring location denoted by a black circle) and wind-stress vectors (light grey arrows) from the ASCAT scatterometer. The scales for these vectors are plotted in the second row. The panel in the third row shows the OSCAR and ADCP currents ( $\text{cm s}^{-1}$ ) during 10 November to 15 December. The ADCP current is from the bin centred at 19 m from the surface. The curves plotted are for the alongshore (solid black) and cross-shore (dashed black) current components from OSCAR and the alongshore (solid grey) and cross-shore (dashed grey) current components from the ADCP. The positive(negative) part of along-shore component of current show that the currents are towards north(south). The sign convention for these current components is as follows: the alongshore (cross-shore) component is positive poleward (onshore) and negative equatorward (offshore). Following Amol et al. (2014), the ADCP data were de-tided using the TASK (Tidal Analysis Software Kit) software (Bell et al., 1998) and filtered with a fourth-order Butterworth filter; the filter used low-passed the hourly data with a two-day cutoff. The vertical black lines mark the period during which the movement of the Filament and Front have been plotted in the first two rows.



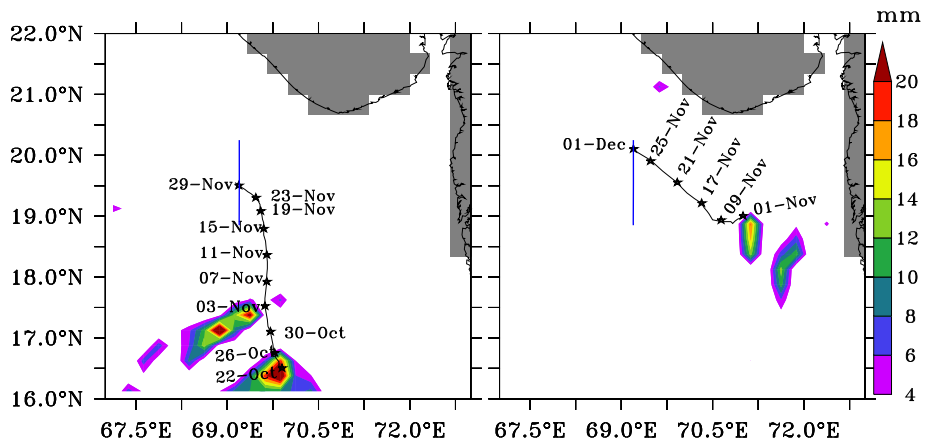


Figure 6: The left (right) panel shows the rainfall in mm from the TRMM TMI on 22 October (1 November). Superimposed on the rainfall is the path, marked by black asterisks, followed by the low-salinity pool of water due to these high-rainfall events. The low-salinity pool in the left panel was advected from (69.90°E, 16.50°N) on 22 October to (69.20°E, 19.55°N) on 29 November and was seen just north of the Filament in the CTD transect (Figure 3). The low-salinity pool in the right panel was advected from (71.20°E, 19.00°N) on 1 November to (69.20°E, 20.20°N), within the Front, on 1 December.

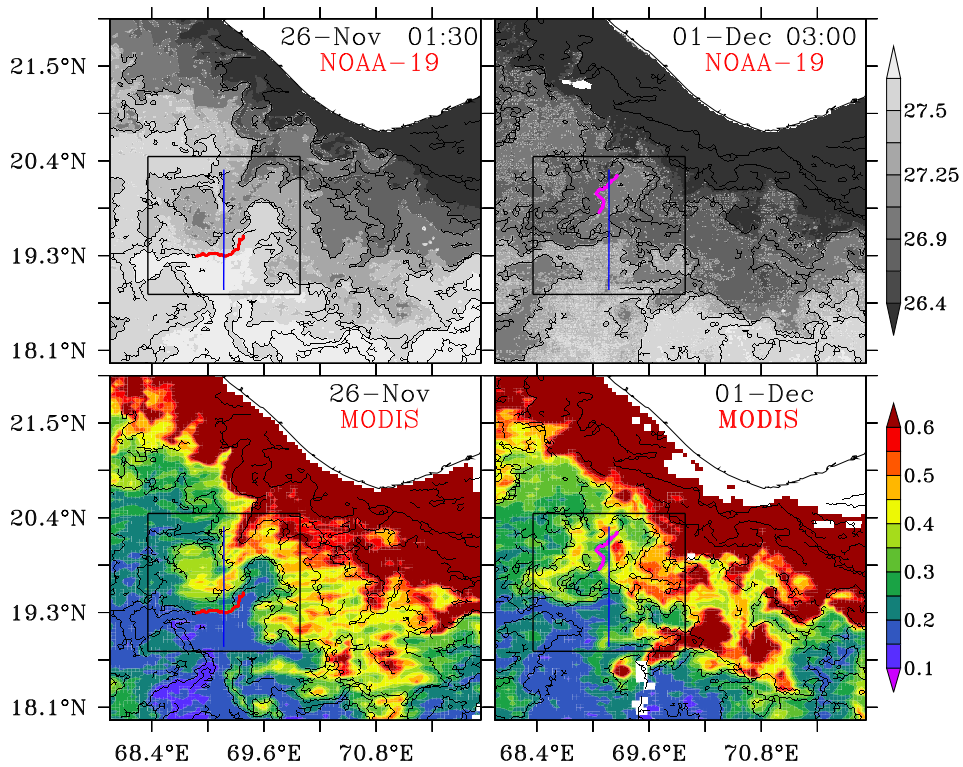


Figure 7: The top (bottom) panels show the SST (chlorophyll) from the NOAA-19 (MODIS Aqua) satellite on 26 November (left) and 1 December (right) in the NEAS. The red (magenta) curve denotes the Filament (Front), the black curves denote other SST fronts, and the black rectangle marks the region shown in Figure 2. The blue line shows the transect mapped during the cruise. Note that most of the SST fronts appear as the boundaries of high-chlorophyll-concentration regimes and that lower SST is associated with the higher chlorophyll concentration.